Disordering of the (111) surface of germanium crystal near its bulk melting temperature

E. G. McRae and R. A. Malic
AT&T Bell Laboratories, Murray Hill, New Jersey 07974
(Received 29 April 1988; revised manuscript received 18 July 1988)

The reversible disordering transition of the Ge(111) surface near 1050 K (160 K below the bulk melting temperature) has been studied by low-energy electron diffraction (LEED). Measurements were made using a position-sensitive detection system with the following characteristics: maximum speed, 10^5 electrons/sec; resolution, 256×256 channels with up to 2^{16} counts per channel. LEED peak and total (integrated) intensities I were recorded for varying electron energy E [$I(E)$ plots] or varying crystal temperature T [$I(T)$ plots]. Angular intensity profiles and intensity contour plots were also recorded. The $I(E)$ plots are interpreted to indicate that layerlike crystalline order is preserved in the transition, up to but possibly not including the outermost double layer. The angular intensity profiles are interpreted to rule out thermal roughening as a disordering mechanism. The ratios of nonspecular beam intensities to the specular beam intensity for $T>1050$ K are found to be incompatible with a surface-melting mechanism like that described by molecular-dynamics (MD) simulations. The $I(T)$ plots exhibit features, such as ranges of positive slope, which cannot be explained by any previously proposed mechanism of surface disordering. The intensity contour plots for T near 1050 K reveal satellite peaks which also have no conventional explanation. A domain-disordering mechanism is proposed to explain the observations qualitatively. In this mechanism, the domains are laterally strained to a depth of one double layer of crystalline Ge(111). The disordering is described as a loss of registry between the strained domains and the substrate. The possible role of intrinsic lateral compressive stress at the Ge(111) surface is discussed with reference to the observations, the disordering mechanism, and relevant MD simulations. Experimental results for Ge crystal films and a theoretical treatment of LEED from strained domains are presented in the Appendixes.

I. INTRODUCTION

A. Background and objectives

The Ge(111) surface undergoes a reversible disordering transition at a crystal temperature T of about 1050 K, which is 160 K below the Ge bulk melting temperature T_m (1210 K). In this paper we describe a low-energy electron diffraction (LEED) investigation of the mechanism of this transition and the nature of the high-temperature state. A preliminary report of this work has been published.[1]

We first became aware of the existence of the transition in the course of observations on the (111) surface of a thin (500 Å) film of Ge grown by molecular-beam epitaxy (MBE) on a Si substrate.[2] When T was increased we noticed an unexpected weakening of the LEED pattern well below T_m. Subsequently we observe the same transition on massive crystal samples as well as on films.[1] This confirmed that the occurrence of the transition is an intrinsic property of the Ge(111) surface and does not depend on alloying or other thin-film property. However, further experiments on films (Appendix A) revealed a weak dependence of the transition temperature on film thickness; for the thinnest films studied, the transition was observed at a lower temperature.

Aside from LEED, there has been one other indication of an anomalous temperature dependence of Ge(111) surface properties near T_m. The sticking coefficient of O_2 at Ge(111) drops precipitously with increasing crystal temperature near 1050 K.[3–5] This effect is not observed for the Ge(100) or Ge(110) surfaces, and is thought to be associated with an especially high value of the sticking coefficient for Ge(111) below 1050 K.[4]

B. Observation of surface disordering by LEED

The observation of a LEED pattern from a crystal surface is evidence that the crystalline order of the substrate persists right up into the surface region sampled by LEED—i.e., the outermost few atom layers. Disordering in the surface region generally causes a decrease of LEED beam intensities. According to kinematical theory, which provides a useful approximate description of the effects of disorder on LEED, disordering along a given direction will weaken a LEED beam to an extent increasing with the momentum-transfer component in that direction. In particular, qualitatively different changes of the distribution of intensity among different beams are brought about by lateral (surface-parallel) disordering as opposed to normal disordering (disruption of layerlike ordering). Lateral disordering does not affect the specular or (00) beam, but weakens the nonspecular beams to an extent which increases with increasing surface-parallel momentum transfer. In most LEED experiments, the normal momentum transfer is relatively large even for higher-index nonspecular beams, so the intensities are typically more sensitive to normal than to lateral disorder.

 ©1988 The American Physical Society

C. Low-temperature structure

Below 573 K, the Ge(111) surface has $c(2\times8)$ periodicity[6–8] with a unit mesh made up of alternating 2×2 and $c(2\times4)$ subunits.[9] The $c(2\times8)$ unit mesh has two identical sites, as evidenced by the systematic weakness of certain LEED beams (the quarter-order beams).[7] The relative positions of the identical sites are in accord with a simple adatom model.[7,9] However, the intensities of the surface peaks observed in Rutherford backscattering (RBS) are not in accord with that model. The observed RBS intensities[10,11] for Ge(111)-$c(2\times8)$ are similar to those for Si(111)-(7×7) surface, in which case they are accounted for by a well-established model[12–15] whose property most relevant to RBS data is the presence of stacking faults in the outermost atom double layer. Thus it seems likely that the Ge(111)-$c(2\times8)$ surface is faulted also. For Si(111)-(7×7) there are periodically alternating faulted and unfaulted triangular areas so that the surface is faulted over half its area. The faulted and unfaulted areas can be distinguished by scanning tunneling microscopy (STM).[13,14,16] An analogous model for Ge(111)-$c(2\times7)$,[17] in which faulted and unfaulted areas alternate with $c(2\times8)$ periodicity, must be rejected for two reasons: first, it does not account for the systematic weakness of the quarter-order LEED beams; second, an extensive search by STM, spanning many $c(2\times8)$ unit meshes, has failed to reveal any feature attributable to boundaries between faulted and unfaulted areas.[18] Among models for Ge(111)-$c(2\times8)$ that incorporate faulting, the only remaining possibility is that the faulted areas are much larger than the $c(2\times8)$ unit mesh. For increasing crystal temperature above 573 K, the $c(2\times8)$ superstructure beams die out in a manner attributable to adatom disordering.[8]

D. Disordering mechanisms

In the search for an explanation of the higher-temperature disordering at the Ge(111) surface, we consider at the outset two general mechanisms of the disordering of the surfaces of solids at temperatures approaching their bulk melting temperatures. These general disordering mechanisms are thermal roughening[19] and surface melting (also called premelting).[20]

The existence of thermal roughening transitions at crystal surface, possibly at temperatures well below T_m, has been anticipated theoretically for a long time.[19] Roughening is the proliferation of atomic steps on the surface, leading to a divergence of the height-height correlation function.[21] There have been experimental indications of the existence of roughening transitions on high-index Cu (Ref. 22) and Ni (Ref. 23) surfaces, at the surfaces of crystalline Ar films,[24] and at the (110) surfaces of Cu (Ref. 25) and Ag.[26]

The idea that the surface of a solid melts at a temperature T below the bulk melting temperature T_m—i.e., that melting is nucleated at surfaces or grain boundaries—has been advanced to explain the nonobservation of the superheating of solids.[20] The macroscopic description of surface melting requires that the sum of the solid-liquid and liquid-vapor interfacial free energies be less than the solid-vapor interfacial free energy, so that a surface will have a tendency to create a liquid layer upon itself.[20] The development of this description,[27,28] as well as of parallel atomistic theory[29] and molecular-dynamics (MD) simulations,[30] has led to the picture in which melting begins in a thin surface layer whose thickness increases with T and diverges at T_m. This should be observable as a continuous disordering transition with a critical temperature T_c equal to T_m.[31] A variety of observations on ice surface[32] and on metal surfaces[33–36] are in accord with the formation of a liquidlike layer whose thickr ss diverges at T_m in accordance with the simplest theoretical expectation.[37]

E. Experimental approach

LEED measurements required in the investigation of disordering at crystal surfaces include measurements of beam intensity (peak intensity or total intensity) as a function of incident electron energy E [$I(E)$ plots] or crystal temperature T [$I(T)$ plots], and the angular distribution of intensity around the center of each beam (intensity contour plots or angular profiles).

The LEED $I(E)$ plot, more commonly called I-V plot, is the standard experimental input to surface structure determination by LEED.[38] No structure determination has been made for a crystal near its melting temperature, but the $I(E)$ plot can give a useful indication of ordering. For example, the presence of Bragg peaks in the $I(E)$ plot is an indication of layerlike ordering near the surface. $I(E)$ plots are also required in conjunction with $I(T)$ plots to discriminate between order-disorder and order-order transitions. A decrease of intensity of a beam for energies corresponding to peaks in the $I(E)$ plot may be attributed to disordering, while a similar decrease for some off-peak energy could result from an $I(E)$ peak shift associated with an order-order transition.

$I(T)$ plots of judiciously chosen values of E provide the clearest LEED indication of the existence and some properties of a disordering transition. It is important to include as many beams as possible, for the reasons indicated in Sec. I B.

The importance of measuring the angular distribution of intensity near the beam center is most obvious with regard to the identification of thermal roughening. The ability of LEED to characterize steps on crystal surfaces on the basis of intensities in the wings of angular profiles is well established.[39–42] Thus the proliferation of steps which constitutes roughening should be detectable.

The requirements outlined above are relatively difficult to meet in the present experiments for several reasons. At high temperatures, intensities can be greatly attenuated because of the Debye-Waller factor.[38] In LEED from Ge, the Debye-Waller factor at 1000 K is about five times smaller than at room temperature, and the thermal diffuse background is somewhat higher. Near T_c for Ge(111) the beam intensities are further reduced by a factor of about 5 because of disordering. Above 1000 K the light emitted from the glowing sample would interfere with conventional LEED detection using a fluorescent screen—a problem that would be difficult to overcome without loss of angular resolving power. Angular resolving power adequate to detect steps that might appear,

e.g., in a roughening transition is an important requirement. In order to make the measurements, we have modified our LEED system incorporating position-sensitive detection to permit automatic recording of $I(E)$ and $I(T)$ plots at enhanced count rates, and we have improved the detection resolution.

II. EXPERIMENTAL METHOD

A. Arrangement

The LEED system (Fig. 1) was basically the same as described previously.[43,44] Inside the ultrahigh vacuum (UHV) envelope it was simpler than the earlier version in that both the position-sensitive detector head (shield grid, channel plates, and resistive anode) and the electron gun were fixed instead of moveable. The scattering angle to the center of the detector was 90°. The active area of the detector subtended 14° at the sample. The electron gun was a standard LEED gun, but when operated at the low gun currents permitted for LEED with position-sensitive detection (about 10^{-11} A) the angular divergence of the beam was relatively small—about 0.3° instead of about 1.0° in conventional operation. The beam departed noticeably from cylindrical symmetry owing presumably to off-center positioning of the filament.

The position-sensitive detection system was basically the same as described previously,[44] but its performance has been enhanced substantially by provision of improved position-computing electronics[45] and of an event-counting memory.[46] The maximum detection rate was 10^5 electrons/sec with 256×256-channel position resolution and 16 bits per channel. The system included edge-gating controls which could be used to limit the x and y coordinates of detection. The system also included a dead-time meter which made it easier to avoid problems associated with saturation. A storage scope was used to monitor the analog output of the detector.

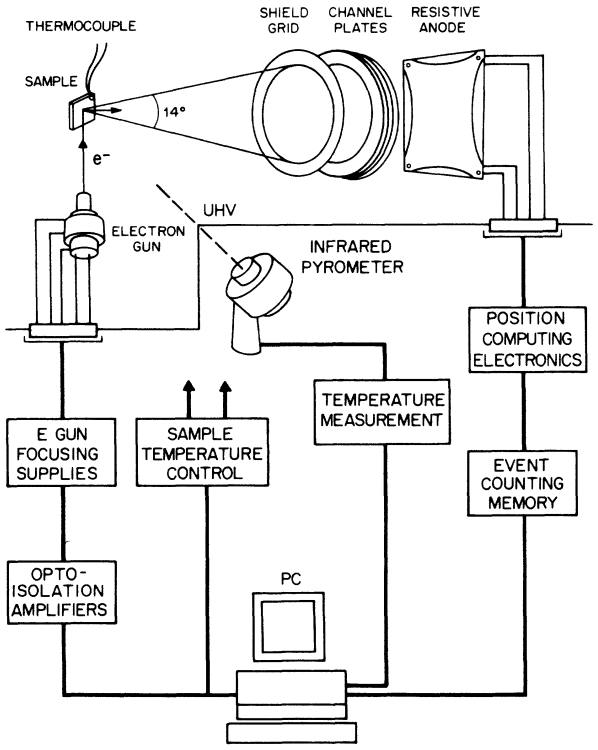

FIG. 1. Schematic indication of the experimental arrangement.

The sample was mounted on a manipulator providing rotation and tilt adjustments. It was heated Ohmically. Its temperature at the position of impingement of the LEED beam was measured in the range 875–1100 K using an infrared pyrometer. As an initial check of the linearity of the internal calibration of the pyrometer, it was confirmed that the output increased smoothly with power dissipated in heating the sample. This is important because some pyrometers employ a coarse piece-wise linear fit to the black-body function. The accuracy and precision of the temperature measurement were 10 and 1 K, respectively.

Measurements were controlled by a personal computer (PC) which was made to vary the electron-gun electrode potentials to maintain focusing while varying the electron energy [$I(E)$ plots] or to vary the sample temperature [$I(T)$ plots]. The detailed operation is described elsewhere.[47]

B. Samples

Our observations were made on Ge crystal samples (n type, Sb doped, 0.01 Ω cm, 12×6×0.25 mm^3). The surface was prepared by sputtering (10^{17} Ne^+ ions/cm, 800 eV, 820 K, normal incidence) and annealing (970 K, 30 min). After this treatment the room-temperature surface was found to be clean and well ordered according to the usual criteria of Auger-electron spectroscopy (AES) and LEED. AES scans at temperature and after each data run showed no impurity above the AES detection limit (about 0.2% of a monolayer). In LEED from room-temperature samples the $c(2\times8)$ pattern was observed against a background low enough to permit easy observation of the quasiforbidden quarter-order beams.[8]

After the sample had been heated a few times to temperatures near the bulk melting temperature (about 1100 K) we noticed evidence of steps in the room-temperature LEED pattern. The pattern did not change upon further temperature cycling. The development of steps was associated with the appearance of slip lines in Normarski micrographs of the surface. We think that the sample was deformed because of inhomogeneous heating. These indications of deformation were made more marked for thinner samples used in preliminary experiments. No steps were observed on the surfaces of Ge films on Si substrates, Appendix A, yet the disordering transition occurred at the same temperature as on massive crystals within error. The results do not depend importantly on crystal deformations or steps.

C. Procedures

The conventions used to designate the crystal orientation and the LEED beams is shown in Fig. 2. All observations were made with a nominal setting $\phi_c = 30°$, but

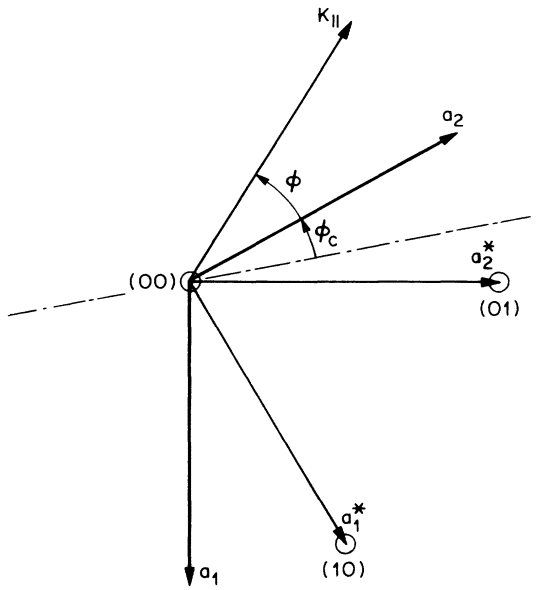

FIG. 2. Designation of net vectors ($\mathbf{a}_1,\mathbf{a}_2$), reciprocal net vectors ($\mathbf{a}_1^*,\mathbf{a}_2^*$), diffraction beams (circles), the surface projection $\mathbf{K}_{\parallel}$ of the incident momentum, the azimuthal angle of incidence ϕ, and the azimuthal angle of orientation of the crystal ϕ_c relative to the apparatus plane (the plane containing the incident beam and the center of the detector). The direction of the dot-dashed line is that of the intersection of the crystal surface and the apparatus plane.

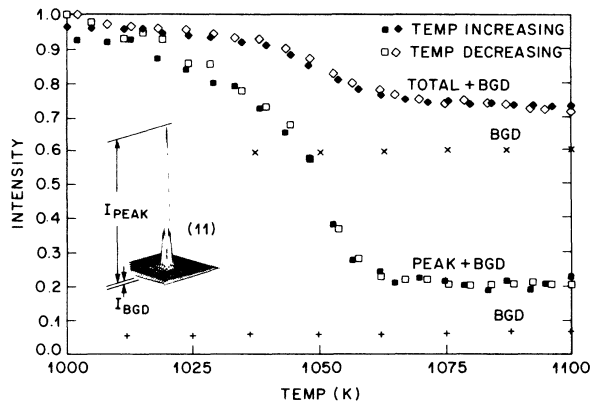

FIG. 3. Raw intensity vs temperature data illustrating measurement procedures. The measurement window and measured quantities are indicated in the inset. The peak intensity I_{peak} is the number of counts/sec in the highest channel, less a background (bgd) intensity I_{bgd} equal to the average counts/sec channel when the beam is just out of the window. The total intensity is the number of counts/sec in a window containing the beam, less the number of counts/sec when the beam is just out of the window. The data points refer to the (11) beam, but the following illustrated properties are common to all beams studied: There is no significant difference between intensities measured with crystal temperature T increasing and T decreasing; the background intensity values increase only very slowly with increasing T; and all intensity values are nearly constant for $T > 1070$ K.

there are small (up to 5°) deviations from this because of the earth's magnetic field and the fields due to Ohmic heating of the sample. These deviations were ignored in specifying LEED incidence conditions.

Essentially similar procedures were followed in making intensity measurements versus E and T, respectively. For measurements versus T the procedure is illustrated in Fig. 3, and may be outlined as follows. Preparatory to beam intensity measurement, the edge-gating controls were set to enclose the beam over the desired range of T. Then, under the control of the PC, T was increased in approximately constant increments. After each increase of T, the position-sensitive intensity measurement was initiated and continued until the number of counts in the highest channel reached a value (typically 10^4) preset to give a desired tradeoff between counting error and accumulation time. At that point the accumulation time (typically 1 min) and the total number counts in the windowed channels (typically 10^7) were stored. When required, the entire digital record of the LEED pattern was also stored at this point, with a view to later display as intensity contour or angular profile plots. When a preset maximum value of T was reached, T was decremented and either the same intensity measurements were done to check reversability or similar measurements were done to determine the background. The background intensity measurement was made the same way as the beam intensity measurement, except in that the edge gating controls were set to just exclude the beam. The peak and total intensities were calculated according to the definitions in the caption of Fig. 3.

In most of the results in this paper, the number of counts in the maximum channel was preset large enough to make the counting errors smaller than 1%. An exception is the angular profile in Fig. 4(f), where the counting error is about 5%. The jitter in the "peak+bgd" plot (e.g., in Fig. 3) is not noise; the width of the beam is only about ten channel spacings, so there is a spurious variation of peak intensity as its impingement position at the detector wanders due to varying stray fields. This could be corrected for by an appropriate interpolation, but this was not done in the present paper. The main difference between the $I(E)$ and $I(T)$ measurement procedure is that for $I(E)$ the electron-gun potentials were varied to maintain optimal focus.[47]

III. RESULTS AND DISCUSSION

A. $I(E)$ plots: Layerlike ordering

LEED $I(E)$ plots for crystals contain peaks corresponding to Bragg reflection conditions.[38] In the case of the (00) beam, the peaks derive mainly from Bragg reflection at discrete layers of atoms parallel to the surface. All the observed (00)-beam $I(E)$ plots for Ge(111) (Fig. 4) contain well-defined peaks, proving that within the sampling depth of LEED there are discrete layers of atoms parallel to the surface for T above as well as below T_c. The sampling depth is roughly $[K_{\perp}''(\text{in})+K_{\perp}''(\text{out})]^{-1}$ which is 5 Å for 70 eV electrons in Ge(111) (notations and values are from Table I). This is between one and

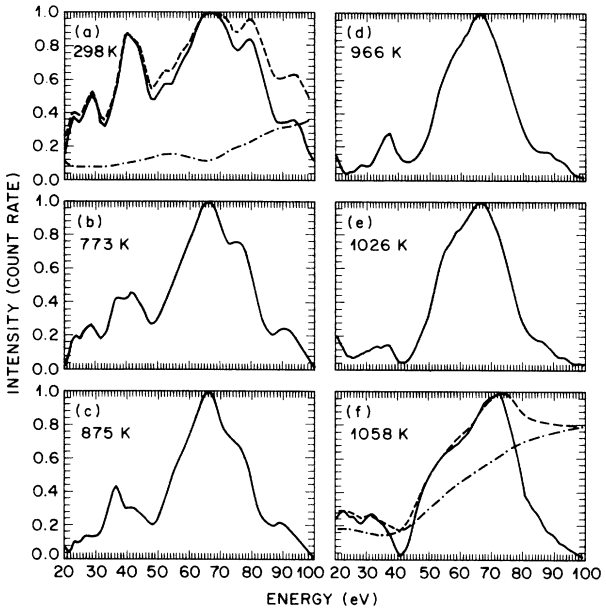

FIG. 4. Dependence of (00) total intensity vs electron energy plots on crystal temperature. Solid lines indicate background-subtracted intensities normalized to unit peak intensity. In panels (a) and (f), the normalized total intensity (dashed lines) and background (dot-dashed lines) are also shown.

two times the double-layer spacing d for Ge(111) at room temperature (3.26 Å). Thus the $I(E)$ plots indicate that with increasing T approaching T_c, layerlike ordering is preserved in at least the second and deeper double layers. [We present evidence further on (Sec. III C) that layerlike ordering is preserved in the outermost double layer as well.] As T increases there are progressive changes in the positions and shapes of the $I(E)$ peaks, especially near 960 K [see Figs. 4 and 7(a), inset]. This could be due to a change of ordered structure (order-order transition) or to disordering of the outermost double layer near 960 K.

B. Angular profiles: Steps and absence of a roughening transition

The LEED pattern had a streaky appearance attributable to steps running predominantly in the direction $\mathbf{a}_1$ (Fig. 2). The angular profiles perpendicular to the streaks were independent of E and became slightly narrower with increasing T.[1] The profiles parallel to the streaks exhibited a strong dependence on E. Figure 5 shows some of these angular profiles for the (00) beam. The streaks show up as shoulders whose position and prominence depend on the phase of interference between electron waves reflected from different step terraces. To describe this interference in the simplest possible way, we consider a strip of the surface of width $2w$, with sides parallel to $\mathbf{a}_1$, containing a single terrace of height h and width w. This model approximately represents a surface with irregularly spaced, alternately up and down steps with average separation w. Exact theoretical treatments of kinematical diffraction from surfaces with steps are available[39–41] but are not used here as our objective is merely to identify the structure in the wings of the beam angular profile as due to steps. The diffraction amplitude near the (00) beam depends on the momentum transfer $\Delta K_\perp$ normal to the terrace, which may be expressed in terms of the surface-parallel momentum transfer $\mathbf{k}$ and the normal and parallel components $K_\perp$ and $\mathbf{K}_\parallel$ of the incident-beam momentum:

$$\Delta K_\perp = K_\perp + (K_\perp^2 - 2\mathbf{K}_\parallel \cdot \mathbf{k} - k^2)^{1/2} . \quad (1)$$

The kinematical expression for the diffraction amplitude is

$$A(\mathbf{k}) = 2[\sin(wa_2^* \mathbf{k}\cdot\mathbf{a}_2)/\sin(\mathbf{k}\cdot\mathbf{a}_2)]\cos(\Delta K_\perp h/2) . \quad (2)$$

In Fig. 5, normalized plots of $|A|^2$ [with k converted to units of angular displacement from the (00)-beam center] are shown together with the observed angular profiles. The correspondence with observation supports the attribution of the shoulders to step parallel to $\mathbf{a}_1$, with step height roughly equal to one double-layer spacing $d = 3.26$

TABLE I. LEED incidence conditions and momenta; (n_1, n_2) beam. Listed are the electron energy E, polar angle of incidence relative to surface normal, θ, azimuthal angle of incidence, ϕ, real part of surface-normal momentum transfer, $\Delta K_\perp'$, imaginary part of surface-normal momentum, ingoing beam, $\Delta K_\perp''$(in), imaginary part of surface-normal momentum, outgoing beam, $\Delta K_\perp''$(out), and magnitude of surface parallel momentum transfer, k. Parameter values: real part of inner potential $V' = 10$ eV, imaginary part of inner potential $V'' = 2$ eV (Ref. 48), unit mesh dimensions $a_1 = a_2 = 4.0$ Å, angle between $\mathbf{a}_1$ and $\mathbf{a}_2 = 120°$, angle between crystal surface direction $\mathbf{a}_2$, and scattering plane equal to 30°.

n_1	n_2	E (eV)	θ (deg)	ϕ (deg)	$\Delta K_\perp'$ (Å^{-1})	$K_\perp''$(in) (Å^{-1})	$K_\perp''$(out) (Å^{-1})	k (Å^{-1})
0	0	69	45	150	6.83	0.08	0.08	0.00
−1	0	63	37	168	6.48	0.07	0.09	1.81
−1	1	73	54	163	6.85	0.09	0.07	1.81
0	−1	80	29	150	7.08	0.06	0.09	1.81
1	−1	90	39	135	7.44	0.06	0.08	1.81
1	0	87	53	138	7.37	0.08	0.06	1.81
1	1	80	71	140	6.77	0.12	0.06	3.14

Å. For example, for $T=300$ K the model accounts for the observations that the shoulders are absent when the in-phase condition $2K_\perp = n\pi$ (n even integer) is satisfied [Fig. 5(c)], and they are relatively prominent and widely spaced when the out-of-phase condition $K_\perp d = n\pi$ (n odd integer) is satisfied [Fig. 5(b)].

The similarity between the angular profiles observed at widely different T values (Fig. 5) rules out the possibility of thermal roughening as the dominant mode of disordering near T_c. As a check on this, Fig. 6 shows angular profiles near an out-of-phase condition, for various values of T. If there were a detectable roughening transition near T_c, this would result in a significant change in the values of h and w required to fit the shoulders. As indicated by the calculated curves [Fig. 6(b)] a 10% change of w or a 3% change of h would be detectable, and the difference between the profiles for $T=300$ K and $T=1058$ K is accounted for by the same increase of h from 3.3 to 3.5 Å as applied in Fig. 5. Actually the profiles for T just above and just below T_c are identical [Fig. 6(a)]. The results of these experiments rule out thermal roughening as the dominant disordering mechanism. The increase of the apparent step height h when T increases from 300 to 1058 K is (6±2)%, which is an order of magnitude greater than the expected increase due to thermal expansion.

C. $I(T)$ plots: Lateral versus normal disordering and absence of surface melting

As mentioned in Sec. I B, disordering in the surface region of a crystal will generally result in a decrease of the intensity of LEED beams. However, a similar decrease

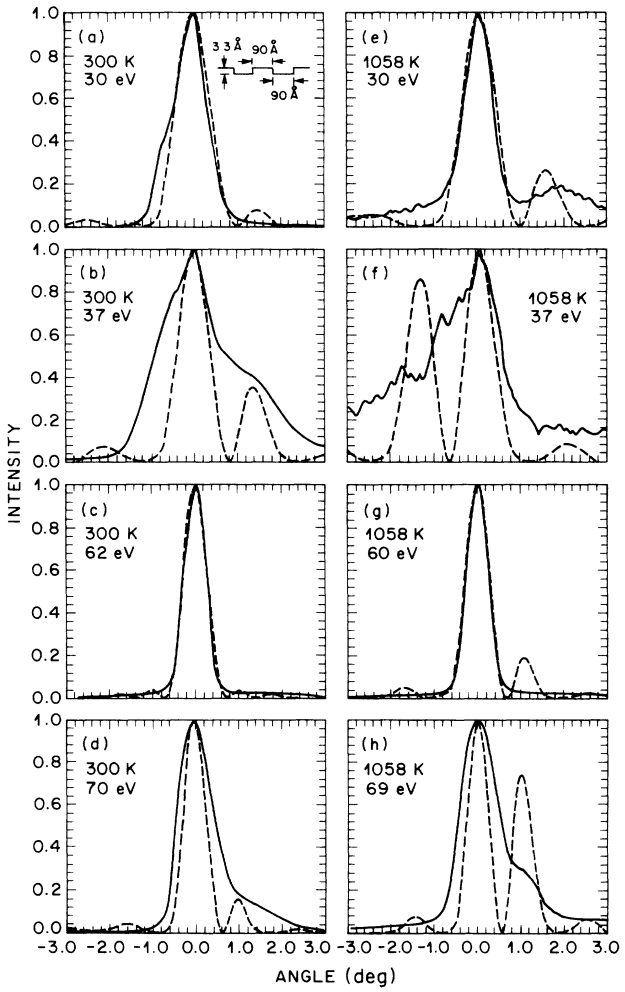

FIG. 5. Dependence of (00)-beam intensity profile on electron energy, for two different values of crystal temperature. The intensity is plotted vs the angular displacement in the (01) direction from the beam center. Solid lines indicate the observed intensities for the temperature and energy values indicated on each panel. Dashed lines indicate kinematical intensities calculated for a model with steps of height h and spacing w [text, Eq. (2)]. The following values of h and w were used: panels (a)–(d) (300 K) $h=3.3$ Å, $w=90$ Å; panels (e)–(h) (1058 K) $h=3.5$ Å, $w=90$ Å.

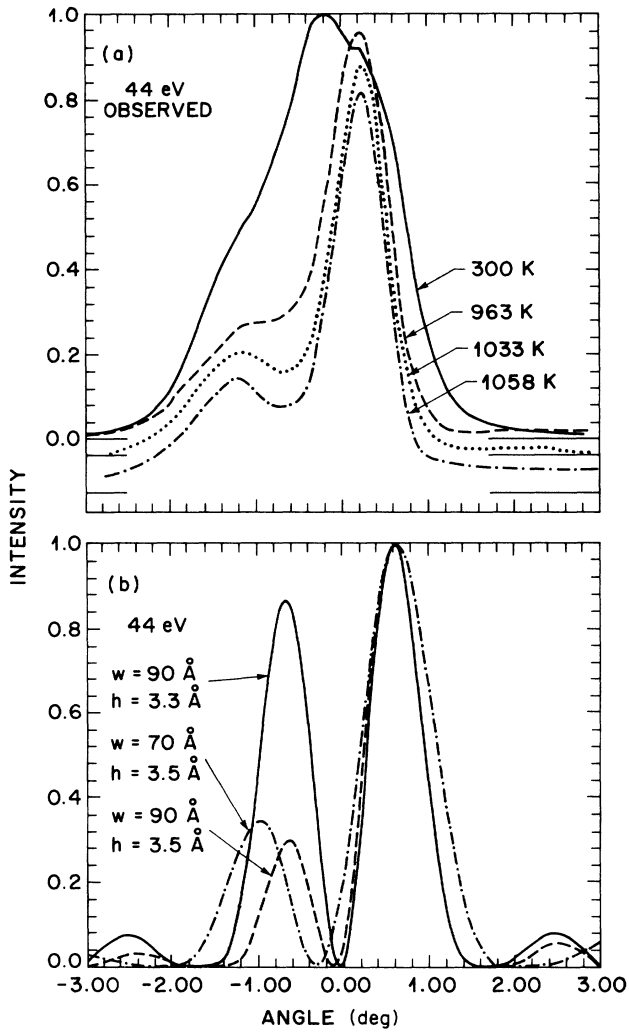

FIG. 6. Dependence of (00)-beam intensity profile on crystal temperature. The intensity is plotted vs the angular displacement in the (01) direction from the beam center. The observed profiles for different temperatures are shown (a) in comparison with the step interference function [text, Eq. (2)] for different step geometries indicated (b).

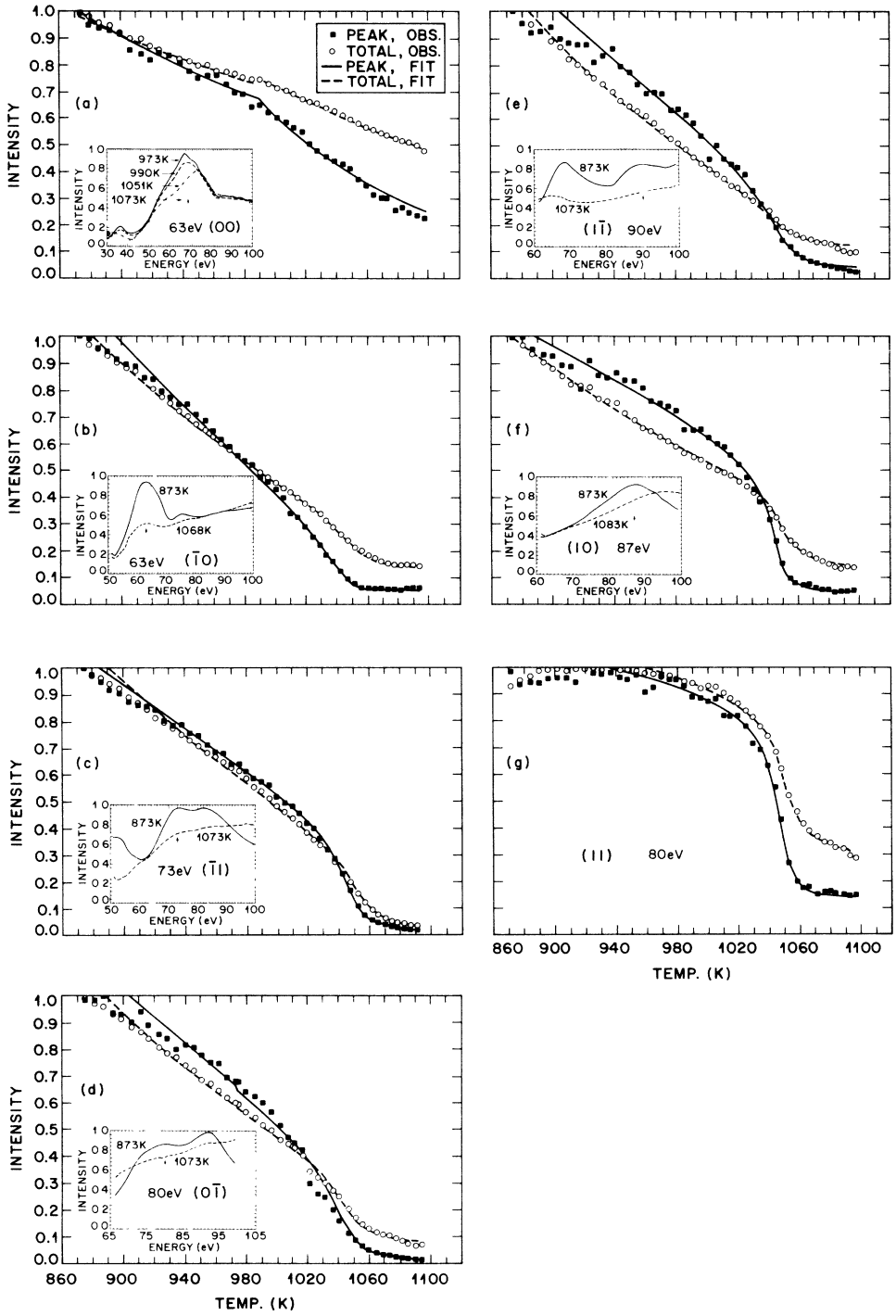

FIG. 7. Beam intensities vs crystal temperature T. The data points indicate measured values of peak and total intensities defined in Fig. 3. The lines are fits using Eqs. (3) and (4) with parameter values given below. The beams are identified in the insets—e.g., panel (a) refers to the (00) beam. Each intensity vs T plot was made with values of incident electron energy E indicated in the inset—e.g., 69 eV for the (00) beam. The energy values correspond to peaks in the intensity vs E plot for the angular incidence conditions required to observe the beam in question (Table I). The insets show total intensity vs E plots, without background subtraction, for values of T above and below the transition temperature near 1050 K. The relevant peaks in these plots are indicated by arrows. The parameter values used in fitting the peak intensities shown in panel (a) were $M'=0.0017\ \mathrm{K}^{-1}$ ($T<T_1=990$ K), $M'=0.0045\ \mathrm{K}^{-1}$ ($T>T_1$). The values used in fitting the peak intensities in the other panels are given in the sequence [$M'(K^{-1})$, β, $a(K)$, $T_c(K)$] as follows: (b) (0.0012, 0.28, 10, 1049), (c) (0.0012, 0.16, 20, 1052), (d) (0.0010, 0.22, 50, 1050), (e) (0.0012, 0.20, 50, 1053), (f) (0.0008, 0.12, 10, 1049), and (g) (0.000, 0.075, 10, 1048). The values used in fitting the total intensities shown in panel (a) were $M'=0.0013$ ($T<T_1$), $M'=0.00195$ ($T>T_1$). The values used in fitting the total intensities in the other panels are given in the same sequence as above as follows: (b) (0.0021, 0.13, 100, 1059), (c) 0.0020, 0.14, 100, 1057), (d) (0.0023, 0.100, 100, 1050), (e) (0.0025, 0.12, 100, 1055), (f) (0.0020, 0.050, 100, 1055), and (g) (0.000, 0.075, 70, 1058).

of intensity might also be observed under fixed LEED incidence conditions (e.g., fixed incidence energy E) as a result of a transition from one ordered structure to another with different LEED characteristics [e.g., shifted peaks in $I(E)$ plots]. To guard against this and observe intensity changes attributable solely to disordering, it is necessary to select incidence conditions corresponding to an intensity maximum with respect to incidence conditions for the ordered structure. Figure 7 shows $I(T)$ plots for incidence conditions corresponding to $I(E)$ maxima for values of T near the low end of the range scanned. The incidence conditions are summarized in Table I. The relevant $I(E)$ plots (total intensity without background subtraction) are shown as insets in Fig. 7. For the (11) beam [Fig. 7(g)], the position of impingement on the detector depended too strongly on E to permit an accurate measurement of $I(E)$. The $I(T)$ measurement was made at 80 eV, which was a visual estimate of the $I(E)$ peak position.[47] Essentially similar $I(T)$ plots were observed for the (11) beam for different values of E in the range 75–90 eV. The $I(T)$ plot for the (01) beam was similar to that for the $(-\bar{1}0)$ beam and is not shown.

In the interpretation of $I(T)$ plots it is generally necessary to distinguish between the effect of disordering and the effect of thermal vibrations as represented by the Debye-Waller factor $\exp(-2M'T)$. According to the Debye-Waller theory, the value of M' in this expression is different for different beams, but is independent of T. In general, this is known to be the case in a good approximation for crystals at temperatures well below their melting temperatures, but might not always hold for surfaces near T_m. Molecular-dynamics (MD) simulations of Ge(111) surface near T_m (Ref. 49) employing the Stillinger-Weber potential[50] for Ge were used to check this. It was found that the key assumption of the Debye-Waller theory, a Gaussian distribution of thermal displacements of atoms from their equilibrium positions, applies right up to T_m.[51]

In the presence of a continuous lateral disordering transition with critical temperature T_c, one expects that with increasing T approaching T_c the intensity of any nonspecular beam should drop to zero like a Debye-Waller factor multiplied by $t^{2\beta}$ where t is the reduced temperature, $t \equiv 1-T/T_c$, and β is a critical exponent. Formulas representing a slight modification of this behavior have been used in attempts to fit the observed $I(T)$ plots as indicated by lines in Fig. 7. For the (00) beam there was no sharp drop of intensity near T_c, so the factor $t^{2\beta}$ was omitted. The formula used to fit the (00) intensity at experimental values T_j of T was

$$I(T_j) \propto \exp(-2M'T_j) , \tag{3}$$

where different constant values of M' were used for T greater and less than a certain value T_x between 950 and 1000 K. The lines in Fig. 7(a) represent Eq. (3) with the values of T_x and of M' shown in the caption. For nonspecular beams the formula used was

$$I(T_j) \propto \sum_{l=-3}^{3} \exp(-2M'T_{j+l})[S(t_{j+l})t_{j+l}^{2\beta}+c] \times \exp\{-[(T_{j+l}-T_j)/a]^2\} . \tag{4}$$

Here S denotes the unit step function, c is a constant included to allow for the observation that the intensity does not fall quite to zero for $T > T_c$, and convolution with the Gaussian simulates the apparent broadening of the transition. The termination of the convolution with $|l|=3$ is arbitrary. Note that T_c must be interpreted as the mean value of a distribution of values of critical temperature of width $2a$. The lines in Fig. 7(b)–(g) represent Eq. (4) with the parameter values indicated in the caption.

The outstanding feature of the results in Fig. 7 is of course the decrease of intensity of nonspecular beams near 1050 K. But it is also noteworthy that the slopes of the $I(T)$ plots are different for T, respectively, below and above a value T_x between 950 and 1000 K. For the (00) beam, the slope for $T < T_x$ is that of Debye-Waller factor with a value of M' corresponding to a surface Debye temperature about two-thirds the bulk Debye temperature.[52] This is the usual slope for a well-ordered crystal surface.[38] For $T > T_x$, the slope is significantly greater than this. Part or perhaps all of the slope change is due to the shift of the peak in the $I(E)$ plot with changing temperature (recall that the measurements were made at fixed E). In order to place an upper limit on that part ΔI of the (00) peak intensity decrease between T_x and T_c attributable to disordering, we have subtracted the estimated effect of the $I(E)$ peak shift as well as the effect of the Debye-Waller factor from the observed decrease of peak intensity I [Fig. 7(a)]. This gives $\Delta I/I < 0.2$. For the nonspecular beams, the data points for $T < T_x$ lie below the fit to the data for $T > T_x$ provided by Eq. (4). In the case of the (11) beam, the intensity increases slightly with increasing T for $T < T_x$, and drops relatively sharply as T approaches T_c. The existence of an upward trend, despite the effect of the Debye-Waller factor, is remarkable.

The main conclusion to be drawn from the results shown in Fig. 7 is that there is a disordering transition near 1050 K, and this disordering is primarily in lateral directions rather than the normal direction. The proof of lateral disordering is that the nonspecular beams are weakened more than the specular one, despite the relatively large values of surface normal compared to surface-parallel momentum transfer for all beams observed. A corollary is that ordering with respect to the surface-normal direction (layerlike ordering) is preserved for $T > T_c$, not only in the second and deeper double layers as deduced from the $I(E)$ data (Sec. III A) but in the outermost double layer as well. A measure of the departure from layerlike ordering is ρ/ρ_0 where ρ is the root-mean-square displacement of the heights of the atoms in a partly disordered layer from their mean height, and ρ_0 is the corresponding thermal root-mean-square displacement. For temperature T, ρ_0 is related to the Debye-Waller exponent $2M'T$ and the surface-normal momentum transfer $K'_\perp$ by $\rho_0=(2M'T)^{1/2}K'_\perp$. If the effect of disordering is to reduce the (00) peak intensity from I to $I-\Delta I$, ρ/ρ_0 has the expression $\{1+(1/2M'T)\ln[I/(I-\Delta I)]\}^{1/2}$. Using $T=1050$ K, $K'_\perp=7$ Å^{-1} (Table I), $2M'T=4$, and $\Delta I/I<0.2$ in accordance with observation, one gets $\rho_0=0.22$ Å and $\rho/\rho_0<1.1$.

The results are incompatible with any mechanism involving a departure from layerlike ordering more pronounced than indicated by a value ρ/ρ_0 equal to 1.1. According to MD simulations for Ge(111),[51] surface melting is such a mechanism. In simulations of the melting of the outermost double layer over a fraction of the area of a Ge crystal near T_m, it was found that the two layers (spacing 0.8 Å in the crystal) merge into one liquidlike layer characterized by a value of ρ/ρ_0 in excess of 2. The experimental results rule out surface melting like that described by MD simulations.

The surface-melting hypothesis was checked also by MD simulations.[49–51] In one set of conditions, the simulations indeed indicated melting of one Ge(111) double layer below T_m. However, this result was obtained only for laterally compressed models; in the absence of stress, there was surface vacancy formation but no melting. Even for stressed models, melting was obtained only above $0.98T_m$ whereas the observed transition is at $0.87T_m$. While the simulations confirm that surface melting of Ge(111) can be induced by compressive stress as previously suggested,[1] they do not support an interpretation of the present results by surface melting.

D. Satellite beams

We have observed satellite beams near integer-order beams in a range of T from 40 K below 20 K above T_c. These observations are illustrated in Fig. 8 by intensity contour plots in which the beams are represented as maxima (arrows). These maxima correspond to very weak satellite spots in a conventional LEED pattern. We have verified that the maxima indicated in Fig. 8 are real (not merely noise) by examining the individual channels in the digital records. In every case the maxima were at least three standard deviations above the neighboring minima. The appearance of the satellite beams in the stated temperature range were consistently reproduced in these experiments, but their precise positions were not reproduced in successive temperature cycles. As illustrated in Figs. 8(b) and 8(c), the peak positions and intensities were found to be strongly dependent on electron energy.

We have previously observed satellite beams in conjunction with other surface phase transitions,[43,53] and we speculate that this might be of frequent occurrence. The effect is a subtle one whose observation probably requires position-sensitive detection or other equally refined method.

E. Strained-domain mechanism of disordering

On the basis of arguments presented in Sec. III C, the LEED observations reported in this paper must be attributed to disordering primarily in lateral directions. The mechanisms of roughening or surface melting, which have been invoked in explanation of other, superficially similar circumstances (Sec. I D) are rejected in the present case because they are thought to involve disordering with respect to the surface-normal direction (Secs.

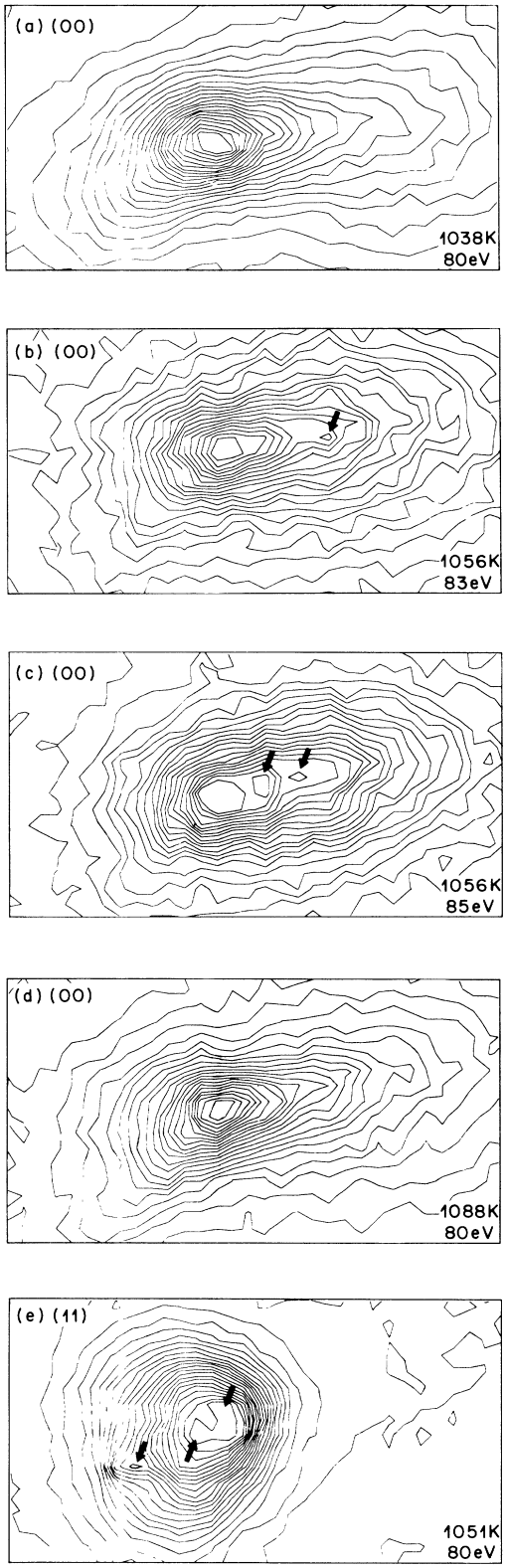

FIG. 8. Intensity contour plots near the (00) beam, panels (a)–(d), and near the (11) beam, panel (e), for values of crystal temperature and of incident electron energy indicated at the bottom right corner of each panel. The arrows point to satellite peaks observed in the temperature range represented. The angular ranges of detection corresponding to the panel dimensions are width, 1.5°; height, 0.8°.

III B and III C). No roughening or surface-melting mechanism can account for the observation of satellite beams above T_c. We propose instead a strained-domain mechanism which chiefly involves lateral disordering, and we discuss how such a mechanism might be able to account qualitatively for the observations.

The basic assumption is that the surface is laterally stressed to an extent increasing with increasing temperature. This stress could result from a difference between the surface and bulk thermal expansion coefficient of the crystal. A laterally stressed surface will tend to take up a natural lateral periodicity different from the bulk lateral periodicity, but this tendency will be opposed by the elastic forces near the surface. The consequences of the competition between periodicities have been worked out in various contexts and for various models of which the best known is that of Frank and Van der Merwe.[54] A general property of idealized models is that for periodicities having a mismatch greater than a critical value, the competition is resolved by the formation of strained domains. These models describe the domain boundaries as dislocations which take up most of the strain. However, for Ge(111) a more plausible picture might be that provided by MD simulations of the laterally compressed crystal for $T > 0.98T_m$.[49] In these simulations, the outermost double layer consists of uniformly-strained crystalline domains with narrow liquidlike boundaries.[51]

According to an approximate kinematical description of the intensity of diffraction from strained domains covering a crystal surface (Appendix B), the intensities of nonspecular beams depend sensitively on the registry between the domains and substrate. The kinematical formulas are given explicitly for a surface monolayer, but the main results apply to a Ge(111) double layer as well. Figure 9 illustrates the kinematical description for an ideal surface (left), for strained domains with perfect registry (center), and for strained domains with imperfect registry (right). In the case of a perfect registry, where the centers of different domains are separated by vectors of the substrate net, there is perfect constructive interference between the diffraction amplitude contributions from different domains, even though the domains themselves may be strained. Any departure from perfect registry will result in some degree of destructive interference, with a corresponding reduction of intensity of nonspecular beams. In the absence of registry, the nonspecular beam intensities will reduce to the sum of intensities from the individual domains. In the kinematical intensity formula [Eq. (B11)] the effect of the loss of registry on the intensity of a nonspecular beam with momentum transfer $2\pi\mathbf{b}_j^*$ is represented approximately by the reduction of the value of the domain interference attenuation factor $|\tilde{X}(2\pi\mathbf{b}_j^*)|^2$ from its maximum value, unity, to zero. For $T > T_c$, where there is no longer any registry, there still remains a contribution to the nonspecular beam intensities from diffraction at the substrate crystal. This substrate contribution is relatively weak because of the attenuation of the incident and diffracted beams in the outermost double layer.

The strained-domain mechanism of surface disordering has two stages: first, the formation of strained domains consisting of the outermost atom layer or layers (Fig. 9, center); second, with increasing T (increasing strain) the loss of registry between the domains and the substrate (Fig. 9, right). The loss of registry is caused by strain. In the absence of strain, each domain atom is at a potential energy minimum with respect to lateral translation. But the atoms of a strained domain are mostly not at these potential minima, so a strained domain can slide across the substrate relatively easily. In wording specifically applicable to Ge(111), the disordering derives from stress-related thermal instability with respect to shuffle displacement of the outermost double layer.[55]

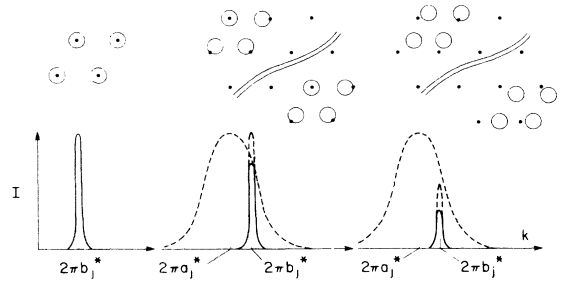

FIG. 9. Top: Hypothetical surface structures with strained domains. Circles indicate surface atoms, dots indicate substrate net points, curved lines indicate a separation between different domains. Bottom: Illustration of the kinematical calculation of diffraction intensity I with respect to lateral momentum transfer $\mathbf{k}$ (solid lines) for the hypothetical structure at top. Left, ideal structure: $I(\mathbf{k})$ is an instrument response function (irf) centered at $2\pi\mathbf{b}_j^*$, where $\mathbf{b}_j^*$ is a substrate reciprocal-net vector. Center, strained domains with perfect registry to the substrate: $I(\mathbf{k})$ is the product of the irf (narrow peak indicated by dashed lines) and the average domain shape transform (broad peak, dashed lines) centered at $2\pi\mathbf{a}_j^*$, where $\mathbf{a}_j^*$ is the domain reciprocal-net vector closest to $\mathbf{b}_j^*$. Right, strained domains with imperfect registry: $I(\mathbf{k})$ is the product of the irf, the shape transform, and a domain interference attenuation factor.

The qualitative variations of intensity indicated kinematically for strained-domain disordering may be illustrated by a simple example. Suppose that a fraction X_0 of the domains are in perfect registry with the substrate, while the remainder are randomly displaced from perfect registry. Then for $k \equiv |\mathbf{k}| \neq 0$, $|\tilde{X}(\mathbf{k})|^2$ is equal to X_0^2. Assuming N domains (N large) whose average domain shape function is Gaussian, $\exp(-r^2/2v^2)$, and whose average area is $2\pi v^2$, so that the average shape transform $\tilde{V}(\mathbf{k})$ is $2\pi v^2\exp(-k^2v^2/2)$. Let γ denote the fractional strain. Apart from a Debye-Waller factor and the factor $|\tilde{W}(\mathbf{k})|^2$ (the effective fraction of the domain area which is uniformly strained, see Appendix B) the peak intensity contribution from the outermost double layer varies approximately in proportion to

$$X_0^2\exp[-(k\gamma v)^2] , \tag{5}$$

where $\mathbf{k}$ takes one of the values $2\pi\mathbf{b}_j^*$ corresponding to the beam in question. The total intensity has an additional, slowly varying contribution from the substrate, and only this contribution remains for $T > T_c$. Specific variations of the values of X_0^2 and of $(\gamma v)^2$ are required to

reproduce the observed variation of intensity of a nonspecular beam with increasing T. To give the decrease of intensity near T_c, X_0^2 must vary like $t^{2\beta}$ (notation of Sec. III C). To give the increase (relative to the Debye-Waller factor) below T_x, $(\gamma v)^2$ must decrease in that range.

The k dependence represented by Eq. (5) derives from the stated assumptions about $\tilde{X}(\mathbf{k})$ and $\tilde{V}(\mathbf{k})$. No theoretical model capable of predicting the dependences on T and k is available. However, the k dependence may be checked by comparing the intensities of beams corresponding to different nonzero values of momentum transfer $2\pi\mathbf{b}_j^*$. If I_j denotes the contribution to the observed intensity of the beam $2\pi\mathbf{b}_j^*$, attributable to the outermost double layer, then according to Eq. (5), $\ln(I_j/X_0^2)$ should be proportional to $|\mathbf{b}_j^*|^2$. Figure 10 shows plots of $I_j(T)$ for j corresponding to the (10) beam (momentum transfer 1.81 Å^{-1}) and the (11) beam ($3.14=\sqrt{3}\times 1.81$ Å^{-1}) together with a decomposition into the factors represented in Eq. (5). The values of $I_j(T)$ were calculated from observed values $I(T)$ indicated in Fig. 7, by subtracting a substrate contribution $I(1060)$, dividing by the Debye-Waller factor $\exp(-2M'T)$ with $M'=0.0017$, and normalizing. Values of $\ln(I_j/X_0^2)$ were calculated assuming $X_0^2=t^{2\beta}$ with $\beta=0.08$ and $T_c=1050$ K. Figure 10 shows that up to about 1000 K, the ratio of the derived values of $\ln(I_j/X_0^2)$ is nearly independent of T as indicated by Eq. (5). Above 1000 K the ratio is highly sensitive to experimental error, e.g., temperature measurement. For $T<1000$ K, the value of the ratio is close to theoretical value, 3, but this apparent agreement might be only coincidental; the derived value is highly sensitive to the Debye-Waller exponent, whose value varies from one beam to another in a way not well understood in the context of LEED.

The above discussion refers only to lateral disordering, and so cannot explain the variation of the (00) intensity.

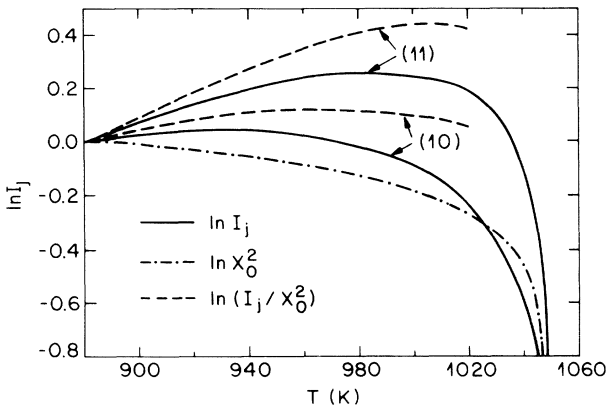

FIG. 10. Plots vs Ge crystal temperature T of $\ln I_j$ (solid lines), $\ln X_0^2$ (dot-dashed line) and $\ln(I_j/X_0^2)$ (dashed lines). I_j denotes the contribution of a Ge double layer to the intensity of the beam indexed j, where j is (10) or (11) as indicated. The values of I_j are derived from a smooth line drawn through experimental peak intensities, Fig. 7, as described in the text. X_0^2 is assumed equal to $t^{2\beta}$ where t is the reduced temperature (see text).

Possibly the change of slope of the $I(T)$ plot [deriving at least partly from changes of the $I(E)$ plot] near T_x is due to surface-normal disordering associated with lateral strain.

The presence of strained domains offers a possible explanation of the presence of satellite beams as well as of the variations of intensity of the main beams. It is very well established that in LEED the multiple scattering between superposed surface structures with different periodicities generally leads to satellite beams.[38] In the strained-domain mechanism described above, the intensities depend mainly on the average properties of the domains. But the sharpest satellite beams likely derive from few, relatively large domains, so it should not be surprising that they are not reproducible in detail in separate temperature cycles.

Notwithstanding these indications of an important role for stress in disordering, the low-temperature structure of the Ge(111) surface (Sec. I B) does not provide any evidence of the intrinsic stress required for this interpretation. The existence of intrinsic stress at Si(111) and Ge(111) has been the subject of previous discussion. The realization that the (7×7) reconstruction of Si(111) might consist of a network of partial dislocations led to the idea that these dislocations have the effect of relieving intrinsic compressive stress, with consequent lowering of surface energy.[56] The observation of strain at Si(111)-(7×7) is consistent with but does not prove the existence of intrinsic compressive stress.[57] Computations[58] deny the existence of significant stress at Si(111). In the case of Ge(111), the application of extrinsic compressive stress due to lattice mismatch in MBE-grown films on Si(111) is known to promote a (7×7) reconstruction similar to that of Si(111).[59] But as noted (Sec. I B), for Ge(111)-c(2×8) there is no evidence of appreciable density of partial dislocations and hence no evidence of intrinsic compressive stress at low temperature.

The strained-domain mechanism offers possible explanations of the main LEED results, but there are two other observations that would be hard to account for in this way. They are the temperature dependences of the O_2 sticking coefficient (Sec. I A) and of step height (Sec. III B).

ACKNOWLEDGMENT

We acknowledge helpful discussions with G. H. Gilmer and M. D. Stiles.

APPENDIX A: DISORDERING OF THE (111) SURFACE OF GERMANIUM CRYSTAL FILMS

Observations were made on Ge films grown by molecular-beam epitaxy on a Si(111)-(7×7) substrate at 550 °C.[60] Except where otherwise mentioned the procedures were the same as described in the text.

The substrate was a low-resistivity (0.05 Ω cm) Si wafer 0.025 cm thick. Films of three different thicknesses—500, 1000, and 5000 Å—were grown on the same wafer. Samples of dimensions 1.0×0.5 cm^2 were prepared to expose equal area of each thickness film. The oxide coating

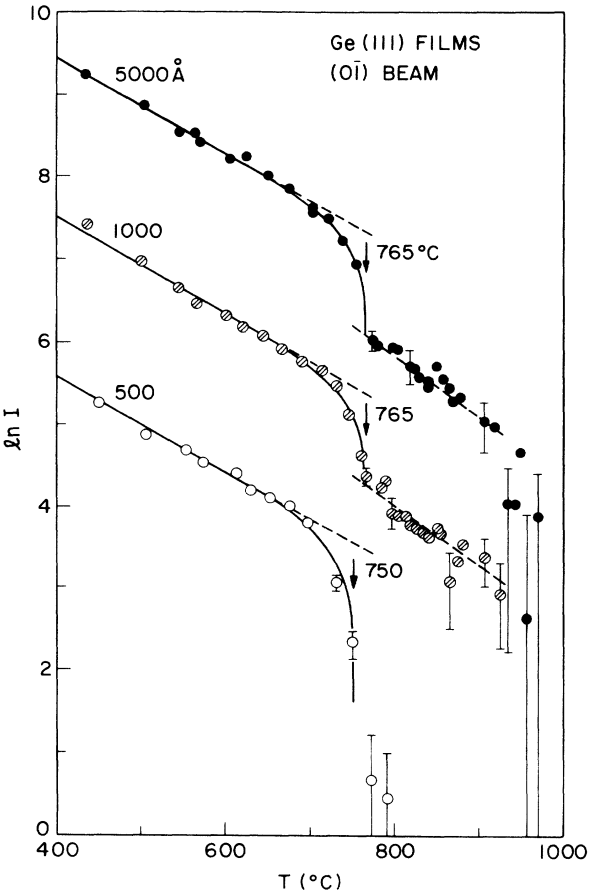

FIG. 11. Peak intensity I for the $(0\bar{1})$ beam vs temperature T for Ge films with the thicknesses indicated. The left scale refers to values of I (counts) for the 5000 Å film. The plots for the other films are shifted down in steps of 2 for clarity. Circles denote data points. Solid lines are calculated by Eq. (4), text, without convolution. The parameter values were $M'=0.0022$, $\beta=0.14$, $c=0$, $a=0$, and the indicated values of T_c. The error bars indicate estimated counting errors.

originally present on the films was removed by sputtering (5×10^{15} Ne^+ ions, 600 V, normal incidence, 500 °C) and annealing (5 min at 600 °C) in an ultrahigh vacuum. After this treatment, the room-temperature film surfaces were pure Ge (<0.02 at. % Si or other impurity) as checked by Auger-electron spectroscopy (AES). In a separate experiment in which the temperature of the films was increased slowly and AES observations were made periodically, no impurities were detected at temperatures up to 800 °C. Si was just detected at the surface of the 500-Å thick film after it had been held at 800 °C for 30 min. After heating at still higher temperatures and cooling, the thinner films were found to have AES and LEED characteristics of specific stable GeSi alloys.[2] However, all observations on disordering were made on pure Ge. The LEED pattern from the 500-Å thick film at room temperature was a superposition of a diffuse $c(2\times8)$ component and a weak, diffuse (7×7) one. The pattern for the 1000-Å thick film was diffuse $c(2\times8)$ while the 5000-Å thick film gave a very sharp $c(2\times8)$ pattern. The LEED patterns gave no indication of steps. The lateral lattice dimensions of three films were compared using a precise LEED method.[61] The dimensions were found to be the same within error (0.05%). Apparently the surface treatment had relieved much of the compressive stress that might have been present originally because of the 4% lattice mismatch between the film and substrate. However, the observation of a (7×7) LEED pattern is indirect evidence of residual stress.[59]

The LEED observations were made using a system described previously,[43] which was an earlier version of the one described in the text. Observations of the disordering transition were made on the $(0\bar{1})$ beam with electron energy 69 eV. The sample surface normal and the incident beam were in the same plane as the $(0\bar{1})$ beam and made angles with it of 32° and 22°, respectively. The sample was heated Ohmically. For each value of power dissipation in the sample, the sample was translated to bring the films of different thickness successively into the incident beam.

The results are summarized in Fig. 11. The peak intensity I followed the normal Debye-Waller temperature dependence up to 700 °C, after which it dropped more rapidly to indicate a disordering transition with apparent critical temperature 750 °C for the 500-Å thick film and 765 °C for the 1000-Å and 5000-Å thick films.

APPENDIX B: KINEMATICAL EXPRESSIONS FOR DIFFRACTION FROM STRAINED MONOLAYER DOMAINS COVERING A CRYSTAL SURFACE

We assume that the domains lie on a flat crystal substrate of indefinitely large lateral extent, and that each domain is laterally strained relative to the substrate. Let $\mathbf{r}$ denote a lateral position on the surface, and let $\mathbf{k}$ denote the surface-parallel momentum transfer in diffraction. Let $U(\mathbf{r})$ denote the response function of the diffraction experiment; $U(\mathbf{r})$ has its maximum value, unity, for $\mathbf{r}=0$, and for increasing $|\mathbf{r}|$ its value decreases at a rate inversely related to the distance over which positional correlations can just be detected experimentally (the coherence-zone diameter). Let N denote the number of domains in the coherence zone.

We assume that the atoms in the domains are identical, and that in each domain there is a central region in which the strain is uniform and the same for all domains. We assume that within each region of uniform strain the atoms are arranged periodically on a net with one atom per unit mesh. Let $\mathbf{a}_1,\mathbf{a}_2$ denote the basic vectors of the net, and let $\mathbf{a}_j$ denote the jth net vector: $\mathbf{a}_j=m_{j1}\mathbf{a}_1+m_{j2}\mathbf{a}_2$, where m_{j1} and m_{j2} are integers. Let $\mathbf{a}_1^*,\mathbf{a}_2^*$ denote the basic vectors of the reciprocal net, so that $\mathbf{a}_1^*\cdot\mathbf{a}_1=1$, $\mathbf{a}_1^*\cdot\mathbf{a}_2=0$, etc., and let $\mathbf{a}_j^*$ denote the jth domain reciprocal-net vector: $\mathbf{a}_j^*=n_{j1}\mathbf{a}_1^*+n_{j2}\mathbf{a}_2^*$, where n_{j1} and n_{j2} are integers. Let $\mathbf{b}_1$, $\mathbf{b}_2$, $\mathbf{b}_j$, $\mathbf{b}_1^*$, $\mathbf{b}_2^*$, and $\mathbf{b}_j^*$ have similar meanings with respect to the substrate periodicity.

We assume that the uniform strain near the center of each domain is small relative to the atom spacing. Let γ denote the fractional uniform strain of the domains relative to the substrate ($\gamma\ll1$), so that corresponding

domain and substrate net vectors are related by $\mathbf{a}_j=(1+\gamma)\mathbf{b}_j$.

We describe the lateral positions of the domains with reference to a hypothetical condition of perfect registry between the strained domains and the substrate: in each domain in perfect registry, there is at least one atom directly above a specific point in the substrate unit mesh such as a substrate atom position. For the pth domain in perfect registry, let $\mathbf{b}_p$ denote the position of the atom satisfying this condition which lies closest to the center of gravity $\mathbf{r}_p$ of the domain (we call $\mathbf{b}_p$ the registry point of the pth domain). In general, all the atoms in a given domain not in perfect registry are shifted by the same amount from the positions they would have had in the same domain in perfect registry. Let $\mathbf{s}_p$ denote this shift for the pth domain.

Let ρ denote the average number of atoms per unit area in the domains. The intensity of diffraction from the domains, relative to the intensity of scattering from a single atom, has the expression

$$I(\mathbf{k})=\left|\sum_{p,j} A_{pj}(\mathbf{k})\right|^2 , \tag{B1}$$

where according to kinematical theory $A_{pj}(\mathbf{k})$ is the Fourier transform of a function whose value is equal to ρ at the position of the jth atom in the pth domain and zero elsewhere:

$$A_{pj}(\mathbf{k})=\rho\int V_p(\mathbf{r}-\mathbf{r}_p)W_p(\mathbf{r}-\mathbf{b}_p-\mathbf{s}_p-\mathbf{a}_j)\exp(i\mathbf{k}\cdot\mathbf{r})d\mathbf{r} . \tag{B2}$$

Here $V_p(\mathbf{r}-\mathbf{r}_p)$ is the shape function of the pth domain; its value is unity if $\mathbf{r}$ lies within the domain boundary, zero otherwise. $W_p(\mathbf{r})$ is the probability that an atom belonging to the pth domain is displaced by $\mathbf{r}$ from the nearest net point. An alternative expression for the intensity may be obtained by using the convolution theorem to express $A_{pj}(\mathbf{k})$ as an integral over momentum transfer, summing over the net indices and substituting the result in Eq. (B1). This expression involves the Fourier transform $\tilde{V}_p(\mathbf{k})$ of $V_p(\mathbf{r})$ (the domain shape transform) and the Fourier transform $\tilde{W}_p(\mathbf{k})$ of $W_p(\mathbf{r})$ (the effective dimension of the uniformly strained region of the domain, expressed as a fraction of the domain dimension). If the domains are roughly the same size and shape, it is a good approximation to replace these functions by average values defined by

$$\tilde{V}(\mathbf{k})=N^{-1}\sum_p \tilde{V}_p(\mathbf{k})\exp[i\mathbf{k}\cdot(\mathbf{r}_p-\mathbf{b}_p-\mathbf{s}_p)] , \tag{B3}$$

$$\tilde{W}(\mathbf{k})=N^{-1}\sum_p \tilde{W}_p(\mathbf{k}) . \tag{B4}$$

We adopt this approximation to obtain through Eq. (B1)

$$I(\mathbf{k})=\left|\rho\sum_j \tilde{V}(\mathbf{k}-2\pi\mathbf{a}_j^*)\tilde{W}(2\pi\mathbf{a}_j^*)\right|^2 \times\left|\sum_p \exp[i\mathbf{k}\cdot(\mathbf{b}_p+\mathbf{s}_p)]\right|^2 . \tag{B5}$$

Equation (B5) expresses the intensity as a product of a factor representing diffraction from an average domain, multiplied by a factor representing the interference between domains.

We express the domain interference function in Eq. (B5) as the product of a factor $N\tilde{G}(\mathbf{k})$ representing the interference among N domains in perfect registry with the substrate, multiplied by a factor $\tilde{X}(\mathbf{k})$ representing the effect of departures from perfect registry. In an approximation similar to that of Eq. (B4), neglecting correlations between domain displacements, the second factor has the expression

$$\tilde{X}(\mathbf{k})=N^{-1}\sum_p \exp(i\mathbf{k}\cdot\mathbf{s}_p) . \tag{B6}$$

In the first factor, $\tilde{G}(\mathbf{k})$ is the Fourier transform of the domain positional pair correlation function detected by the diffraction experiment:

$$G(\mathbf{r})=N^{-1}U(\mathbf{r})\rho\sum_{pq}\delta(\mathbf{r}-\mathbf{b}_p+\mathbf{b}_q) . \tag{B7}$$

The approximation $\rho\approx|\mathbf{b}_1\times\mathbf{b}_2|^{-1}$ is used. The double summation in Eq. (B7) may be replaced by N plus N times a single summation, over the N_b substrate net points in the coherence zone, of terms like $p_j=P(\mathbf{r})\delta(\mathbf{r}-\mathbf{b}_j)$: p_j denotes the conditional probability of a domain having its registry point at $\mathbf{b}_j$, given that a different domain has its registry point at the origin. By making these substitutions in Eq. (B7) and Fourier transforming, we get for the interference function for domains in perfect registry

$$\left|\sum_p \exp(i\mathbf{k}\cdot\mathbf{b}_p)\right|^2=N\tilde{G}(\mathbf{k}) =N+N\rho\sum_j\int\tilde{U}(\mathbf{k}-\mathbf{k}'-2\pi\mathbf{b}_j^*) \times\tilde{P}(\mathbf{k}')d\mathbf{k}' . \tag{B8}$$

We consider specific kinds of ordering of the domains that might apply for sufficiently large values of N ($N>10$). As no domain is likely to have its registry point within an average domain diameter from that of another domain, $P(\mathbf{r})$ has the approximate expression

$$P(\mathbf{r})=D(\mathbf{r})[1-V(\mathbf{r}/2)] , \tag{B9}$$

where $D(\mathbf{r})$ is slowly varying. Long-range ordering of domain positions is represented by modulations of $D(\mathbf{r})$. In the absence of any modulation, we get for the domain interference function

$$\left|\sum_p \exp(i\mathbf{k}\cdot\mathbf{b}_p)\right|^2=N+N(N-1)\sum_j\tilde{U}'(\mathbf{k}-2\pi\mathbf{b}_j^*) , \tag{B10}$$

where $\tilde{U}'(\mathbf{k})$ stands for $\tilde{U}(\mathbf{k})-4\tilde{V}(2\mathbf{k})$, and $D(\mathbf{r})$ has been replaced by its average value $(N-1)/[U'(0)\rho]$. In the presence of modulation with wave vector $2\pi\mathbf{c}^*$, the result is the same as Eq. (B10) except for additional terms with $\mathbf{b}_j^*\pm\mathbf{c}^*$ in place of $\mathbf{b}_j^*$.

For sufficiently large values of N ($N>10$), the domain shape transform $\tilde{V}(\mathbf{k})$ is much broader than $\tilde{U}(\mathbf{k})$. Because of this, and the assumption that the strain is small ($\gamma\ll1$), the intensity expression for $\mathbf{k}\approx2\pi\mathbf{b}_j^*$ obtained by substituting Eq. (B10) into Eq. (B5) is approximately

$$I(\mathbf{k})=N\rho^2|\tilde{W}(2\pi\mathbf{b}_j^*)|^2\,|\tilde{X}(2\pi\mathbf{b}_j^*)|^2[\,|\tilde{V}(\mathbf{k}-2\pi a_j^*)|^2+(N-1)|\tilde{V}(2\pi\mathbf{b}_j^*-2\pi\mathbf{a}_j^*)|^2\,\tilde{U}'(\mathbf{k}-2\pi\mathbf{b}_j^*)]\ . \tag{B11}$$

[1]E. G. McRae and R. A. Malic, Phys. Rev. Lett. **58**, 1437 (1987). The beam labeled (01) is $(0\bar{1})$ in the present paper.

[2]E. G. McRae and R. A. Malic, Surf. Sci. **165**, 191 (1986).

[3]R. F. Lever, Surf. Sci. **9**, 370 (1968).

[4]R. F. Lever and H. R. Went, Surf. Sci. **19**, 435 (1970).

[5]A. A. Frantsuzov and N. I. Makrushin, Surf. Sci. **40**, 320 (1973).

[6]D. J. Chadi and T.-C. Chiang, Phys. Rev. B **23**, 1843 (1981).

[7]W. S. Yang and F. Jona, Phys. Rev. B **29**, 899 (1984).

[8]R. J. Phaneuf and M. B. Webb, Surf. Sci. **164**, 167 (1985).

[9]R. S. Becker, J. A. Golovchenko, and B. S. Schwartzentruber, Phys. Rev. Lett. **54**, 2678 (1985).

[10]R. J. Culbertson, Y. Kuk, and L. C. Feldman, Surf. Sci. **167**, 127 (1986).

[11]A recent challenge of the results of Ref. 10, if sustained, would make it unnecessary to consider faulting of Ge(111): P. M. J. Mareé, K. Nakagawa, J. F. van der Veen, and R. M. Tromp, Phys. Rev. B **38**, 1585 (1988).

[12]K. Takayanagi, Y. Tanishiro, M. Takahashi, and S. Takahashi, Surf. Sci. **164**, 367 (1985).

[13]R. S. Becker, J. A. Golovchenko, E. G. McRae, and B. S. Schwartzentruber, Phys. Rev. Lett. **55**, 2028 (1985).

[14]R. M. Tromp, R. J. Hamers, and J. E. Demuth, Phys. Rev. B **34**, 1388 (1986).

[15]I. K. Robinson, W. K. Waskiewicz, P. H. Fuoss, J. B. Start, and P. A. Bennett, Phys. Rev. B **33**, 7013 (1986).

[16]G. Binnig, H. Rohrer, C. Gerber, and E. Weibel, Phys. Rev. Lett. **50**, 120 (1983).

[17]K. Takayanagi and Y. Tanishiro, Phys. Rev. B **34**, 1034 (1986).

[18]R. S. Becker, B. S. Schwartzentruber, and J. S. Vickers (unpublished).

[19]For a review, see J. D. Weeks, in *Ordering in Strongly Fluctuating Condensed Matter Systems*, edited by T. Riste (Plenum, New York, 1980).

[20]For a review, see J. K. Kristensen and R. M. J. Cotterill, Philos. Mag. **36**, 437 (1977); R. M. J. Cotterill and J. K. Kristensen, *ibid.* **36**, 453 (1977).

[21]The discussion applies also to the proliferation of steps on a flat surface (preroughening), which has also been discussed recently: K. Rommelse and M. den Nijs, Phys. Rev. Lett. **59**, 2578 (1987).

[22]J. Lapujoulade, B. Salanon, and D. Gorse, in *The Structure of Surfaces*, edited by M. A. Van Hove and S. Y. Tong (Springer, New York, 1985), p. 176; J. Villain, D. Grempel, and J. Lapujoulade, J. Phys. F **15**, 809 (1985).

[23]M. den Nijs, E. K. Riedel, E. H. Conrad, and T. Engel, Phys. Rev. Lett. **55**, 1689 (1985); **57**, 1279 (1986).

[24]D. Zhu and J. G. Dash, Phys. Rev. Lett. **57**, 2959 (1986).

[25]S. G. J. Mochrie, Phys. Rev. Lett. **59**, 304 (1987).

[26]G. A. Held, J. L. Jordan-Sweet, and P. M. Horn, Phys. Rev. Lett. **59**, 2075 (1987).

[27]R. Lipowsky and W. Speth, Phys. Rev. B **28**, 3983 (1983).

[28]R. Lipowsky, Ferroelectrics **73**, 69 (1987).

[29]L. Pietronero and E. Tosatti, Solid State Commun. **32**, 255 (1979).

[30]J. Q. Broughton and G. H. Gilmer, J. Chem. Phys. **79**, 5105 (1983); **84**, 5741 (1986).

[31]There is a recent theoretical prediction of "blocked" surface melting in which the thickness of the molten layer does not diverge, but levels off at a finite value in a transition with $T_c < T_{in}$: A. Trayanov and E. Tosatti, Phys. Rev. Lett. **59**, 2207 (1987).

[32]U. Nakaya and A. Matsumoto, J. Colloid Sci. **9**, 41 (1954); J. Clifford, Chem. Commun. **323**, 880 (1967); V. Kvlividze, V. Kiselev, A. Kurzaev, and L. Uschakova, Surf. Sci. **44**, 60 (1974); S. Valeri and S. Montovani, J. Chem. Phys. **69**, 5207 (1978); I. Golecki and C. Jaccard, Phys. Lett. **63A**, 374 (1977); D. Beaglehole and D. Nason, Surf. Sci. **96**, 357 (1980).

[33]J. W. M. Frenken and J. F. van der Veen, Phys. Rev. Lett. **54**, 134 (1985).

[34]B. Pluis, A. W. D. van der Gon, J. W. M. Frenken, and J. F. van der Veen, Phys. Rev. Lett. **59**, 2678 (1987).

[35]P. H. Fuoss, L. J. Norton, and S. Brennan (unpublished).

[36]K. C. Prince, U. Breuer, and H. P. Bonzel (unpublished).

[37]Some pioneering LEED experiments, R. M. Goodman and G. A. Somorjai, J. Chem. Phys. **52**, 6324 (1970), failed to reveal surface melting on the surfaces of Refs. 33–36, but the ability of LEED to detect surface melting has been demonstrated recently (Ref. 36).

[38]J. B. Pendry, *Low Energy Electron Diffraction* (Academic, London, 1974); M. A. Van Hove, W. H. Weinberg, and C.-M. Chen, *Low Energy Electron Diffraction* (Springer, New York, 1986).

[39]M. Henzler, Surf. Sci. **73**, 240 (1978); K. D. Gronwald and M. Henzler, *ibid.* **117**, 180 (1982).

[40]T.-M. Lu and M. G. Lagally, Surf. Sci. **120**, 47 (1982).

[41]C. S. Lent and P. I. Cohen, Surf. Sci. **139**, 121 (1984); P. R. Pukite, C. S. Lent and P. I. Cohen, *ibid.* **161**, 39 (1985).

[42]K. D. Gronwald and M. Henzler, Surf. Sci. **117**, 180 (1982).

[43]E. G. McRae and R. A. Malic, Surf. Sci. **148**, 551 (1984).

[44]E. G. McRae, R. A. Malic, and D. A. Kapilow, Rev. Sci. Instrum. **56**, 2077 (1985).

[45]Surface Science Laboratories, Palo Alto, California.

[46]Erbtec Engineering Inc., Boulder, Colorado.

[47]R. A. Malic, Rev. Sci. Instrum. **59**, 1951 (1988).

[48]Value corresponding to the electron escape depth for Ge crystal: H. Gant and W. Monch, Surf. Sci. **105**, 217 (1981).

[49]M. H. Grabow and G. H. Gilmer, Surf. Sci. **194**, 333 (1988).

[50]F. H. Stillinger and T. A. Weber, Phys. Rev. B **31**, 5262 (1985).

[51]E. G. McRae, J. M. Landwehr, J. E. McRae, G. H. Gilmer, and M. H. Grabow, following paper, Phys. Rev. B **38**, 13 178 (1988).

[52]The Debye temperature for the Ge crystal is 290 K: B. W. Batterman and D. R. Chipman, Phys. Rev. **127**, 609 (1962).

[53]E. G. McRae and R. A. Malic, Surf. Sci. **177**, 53 (1986).

[54]For a review, see P. Bak, Rep. Prog. Phys. **45**, 587 (1982).

[55]In the context of diamond-lattice distortions, the word shuffle refers to displacement of at least one entire (111) double layer in a direction parallel to the (111) plane.

[56]E. G. McRae, Phys. Rev. B **28**, 2305 (1983).

[57]I. K. Robinson, W. K. Waskiewicz, P. H. Fuoss, and L. J. Norton, Phys. Rev. B **37**, 4325 (1988).
[58]D. Vanderbilt, Phys. Rev. Lett. **59**, 1456 (1987).
[59]H.-J. Gossmann, J. C. Bean, L. C. Feldman, E. G. McRae, and I. K. Robinson, Phys. Rev. Lett. **55**, 1106 (1985).
[60]J. C. Bean, L. C. Feldman, A. T. Fiory, S. Nakahara, and I. K. Robinson, J. Vac. Sci. Technol. A **2**, 436 (1984). The samples used in this work were provided by J. C. Bean.
[61]E. G. McRae and R. A. Malic, Surf. Sci. **163**, L702 (1985).